Vibration Analysis and Development of a Submersible Ultrasonic Transducer for an Application in the Inhibitory Activity of Pathogenic Bacteria

KAMONWAN SRATHONGHUAM[1], BENJAMAPORN WONGANU[2],
WUTTHIKRAI BUSAYAPORN[3], AND JATUPORN THONGSRI[1]
[1]Computer Simulation in Engineering Research Group, College of Advanced Manufacturing Innovation, King Mongkut's Institute of Technology Ladkrabang, Bangkok 10520, Thailand
[2]Department of Biotechnology, Faculty of Applied Science, King Mongkut's University of Technology North Bangkok, Bangkok 10800, Thailand
[3]Synchrotron Light Research Institute (Public Organization), Nakhon Ratchasima 30000, Thailand

Corresponding author: Jatuporn Thongsri (jatuporn.th@kmitl.ac.th)

ABSTRACT Development of a new generation of a submersible ultrasonic transducer (SUT) using vibrational analysis aimed for higher efficiency and inhibitory activity of pathogenic bacteria has been presented. The SUT with a dual-stepped shape of front mass and PZT8 transducer working at 50W, 110V, 50 kHz has been examined by the plate counting method. It was found that the SUT could inhibit pathogenic bacteria, e.g., *Escherichia coli*, *Salmonella typhi*, *Staphylococcus epidermidis*, and *Staphylococcus aureus*. For the vibrational analysis, the results were derived from structural and acoustic simulations using harmonic response analysis (HRA) in ANSYS software. In the structural simulation, the results showed a natural frequency and total deformations both inside and outside of the original SUT corresponding to the results measured by a laser doppler vibrometer. The acoustic simulation, set up as an actual operation at different depths from the water surface, has been applied. The HRA revealed various distributions of acoustic pressure. For further distances away from the SUT, the acoustic pressure decreased. When the SUT has been submerged deeper into the media, the acoustic pressure becomes larger at positions close to the bottom of the tank. This discovery is consistent with power concentration measurement. For the development of the SUT, this research proposed other 5 models as the candidate to be investigated. The results from the acoustic simulation confirmed that the different shapes of the front mass provided different acoustic pressure distributions. The wider head of the front mass in the modified dual-stepped shape generated the highest acoustic pressure and was fully distributed through an all-over cleaning tank. Therefore, this proposed model is suitable for industrial commercialization and possesses the inhibitory activity of pathogenic bacteria.

INDEX TERMS Acoustic pressure, finite element method, harmonic response analysis, pathogenic bacteria, piezoelectric transducer, ultrasonic cleaning, vibration analysis.

I. INTRODUCTION

Ultrasonic Transducer (UT) is an electronics device that transforms electricity into vibration in the range of 20-200 kHz transmitted through media for such applications. For example, UT has been used in welding machines [1], cell disruptors [2], and cleaning machines [3]–[7]. For the

cleaning purpose, UT can be divided into two types of operation: Outer Ultrasonic Transducer (OUT) and Submersible Ultrasonic Transducer (SUT), as shown in Fig.1(a) and (b), respectively. For OUT type, UT will be installed outer of the cleaning area. Hence the UTs will not directly contact the liquid. In contrast, the UTs of the SUT type will be directly submerged into the cleaning area in liquid. At present, the SUT type draws high demand because of its compact size and high mobility. Moreover, it can
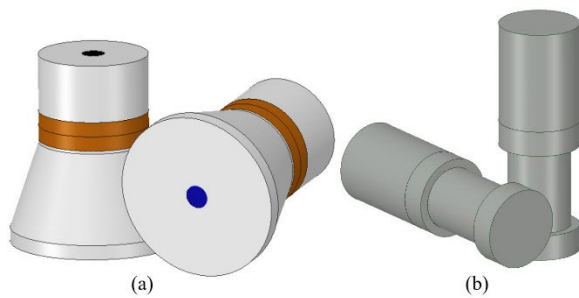
The associate editor coordinating the review of this manuscript and approving it for publication was Agustin Leobardo Herrera-May.

FIGURE 1. Schematic drawing of (a) Outer ultrasonic transducer (OUT) and (b) Submersible ultrasonic transducer (SUT).

be cooperated with the other UTs at different frequencies to form a multi-frequency ultrasonic cleaning tank. These multi-frequency ones can perform high cleaning efficiency for complex-shaped objects such as jewelry, accessories, and electronics devices [6]. Furthermore, the cleaning with an ultrasonic wave at 20-45 kHz for 1-10 mins of sonication time has been proven to inhibit the growth of pathogenic microorganisms in fruits and vegetables. Therefore, this application has been widely utilized in the food industry and household level [8]–[11].

Thailand is one of the major countries of cleaning machine manufacturers in Southeast Asia. Thus, research for cleaning machine development is one of the main topics in this field. However, most studies to develop this technology mainly relied on empirical research on time and budget consumption. Therefore, a proper methodology that reduces the time and budget would be highly needed. Computational simulation has been introduced here as it is such a practical methodology that can be performed to predict the result of the development of the cleaning machine with much less time and expense. Adopting the computer simulation into the development of the cleaning machine can be clearly categorized into two parts: 1) structural simulation, especially on the UTs, and 2) acoustic simulation, especially on the cleaning tank or process. For the structural simulation, as general UTs combined with 3 components as front mass, piezoelectric (PZT), and back mass, the manufacturers commonly focus on using modal analysis to design and develop the front mass to reach its natural frequency and mode's shape consistent with the objective of the applications. Ordinary design of the front mass can be in the shape of hollow [12], stepped, cylindrical, conical, and exponential horns [12]–[16]. The manufacturers commonly use PZT4 and PZT8 as the main materials for the piezoelectric part to originate mechanical vibration. It would be noted that these two materials provide identical vibration from the different electrical properties. Moreover, the PZT8 has been used in devices that require higher durability than the PZT4 [17]–[20]. However, all mentioned technology in previous studies [1]–[20] cannot provide satisfactory industrial cleaning. The produced cavitation still did not fully cover the industrial grade's tank even though there are several UTs installed. For the acoustic simulation, the manufacturers

commonly use the finite element approach such as harmonic response analysis (HRA) to figure the positioning of the UTs which perform the necessary criteria of the cleaning process according to the customers' needs [3]–[7]. In addition, for the cleaning machines included a particle eliminated system, the computational fluid dynamics (CFD) may be applied to find outflow rate, flow direction, shapes, and locations of inlet and outlet. The results were optimized to achieve a high cleaning process efficiency to prevent recontamination of the products [6]. It can be noticed that in [3]–[7] the research relied on the commercial UTs using acoustic simulation which gave rise to the limitation of the cleaning efficiencies. Therefore, if the computational simulation has been employed to develop the specially designed UTs suit to the specific utilization, the efficiency of the cleaning process certainly is increased. Finally, it can be briefly concluded that to develop the SUT for the purpose of high cleaning efficiency and inhibiting the pathogenic bacteria, the computational simulation must be carried out both in structural and acoustic stimulations, simultaneously to reach the complete, accurate and practical results.

In this article, the vibration of original UTs at 50 kHz has been investigated as it can be used as based knowledge of the development of the next model of SUT with higher cleaning efficiency and inhibiting such species of pathogenic bacteria. The computer simulation covered both structural and acoustic simulations using the HRA, consequently. The results can express the SUT's vibration behavior while performing the cleaning process and prove their reliability with the experimental results using Laser Doppler Vibrometer (LDV), power concentration measurement, and plate counting method. All mentioned results will be analyzed and used for the design of a new model of the SUT. The expected outcome of this research can be noted as the knowledge of the behavior of SUT vibration, methodology, and the newly designed SUT with higher efficiency of cleaning and inhibiting the pathogenic bacteria. There is no other research with this kind of simulation yet.

II. HARMONIC RESPONSE ANALYSIS (HRA)
The HRA here will be categorized into (1) structural simulation and (2) acoustic simulation, which have been approached with different equations.

A. STRUCTURAL SIMULATION
Natural frequency, deformation, and amplitude of vibration provided by SUT can be derived as in (1) [5], [6], [21];

$$\left(-\omega^2[M] + j\omega[C] + [K]\right)\{u\} = \{F\} \tag{1}$$

where ω is an angular frequency, $[M]$ is a structural mass matrix, $[C]$ is a structural damping matrix, $[K]$ is a structural stiffness matrix, $\{u\}$ is a nodal displacement vector, and $\{F\}$ is a load vector.

B. ACOUSTIC SIMULATION

The natural frequency of oscillating bubble (f_o) describing the relation between the fluid density (ρ) and the surface tension (σ) generating the cavitation is given by [22].

$$f_0 = \frac{1}{2\pi} \sqrt{\frac{3\gamma P_\infty}{\rho R_0^2} - \frac{2\sigma}{\rho R_0^3}} \tag{2}$$

where P_∞ is the ambient pressure, γ is the specific heat ratio, R_0 is the bubble size resonance.

In (2), manufacturers of ultrasonic cleaners know that the higher rate of cavitation effect occurs at high f_0. On the other hand, at low f_0 the cavitation bubble is more challenging to occur.

The transient bubble's radius (R_t) describes the bubbles' size in terms of frequency (f) and relative transient threshold pressure (P) is [23].

$$R_t = \begin{cases} \frac{0.3}{f} \left(\frac{P_\infty}{\rho}\right)^{1/2} \left(\frac{P-1}{\sqrt{P}} \left(1+\frac{2}{3}(P-1)\right)^{1/3}\right) & for\ P \geq 11 \\ \frac{0.13}{f} \left(\frac{P_\infty}{\rho}\right)^{1/2} \left(\left(\frac{2}{3}(P-1)\right)^{1/3}\right) \\ & for\ P \leq 11 \end{cases} \tag{3}$$

where f is the driving frequency. P_t is the transient threshold pressure, and $P = P_t/P_\infty$.

The meaning of (3) in the manufacturers' perception is that the ultrasonic cleaner with higher f generates a tiny bubble size than the lower f. For a simple task, (2) and (3) can estimate the frequency and cavitation rate appropriate to obtain the bubbles' size corresponding to the particle to be cleaned or microorganisms' size to be growth inhibition. As the efficiency of cleaning and inhibition depends on the cavitation effect related to the distribution and intensity of acoustic pressure (p). In a simple domain such as the case of a wave with constant frequency and velocity propagates into media with steady density and has a single domain (without interface), p can be easily derived from (3), which is a second-order linear partial differential equation mentioned in [3]–[7] as follow;

$$\nabla \cdot (\frac{1}{\rho} \nabla \cdot p) - \frac{\omega^2}{\rho c^2} p = 0 \tag{4}$$

where p is the acoustic pressure, and c is the acoustic velocity.

In addition to the linear wave equation of (4), there are also nonlinear wave equations with different forms depending on the inventor with different applications [24], [25]. For example, Burger's equation is for acoustic and hydrodynamic waves such as streaming and finite-amplitude effects. Fisher's equation is for heat and mass transfer, population dynamics, ecology. Hopf's equation is for gas dynamics and traffic flow. Cubic Schrödinger and Sine Gordon equations are for various areas of physics, nonlinear optics, superconductivity, and plasma models.

Unfortunately, the SUT submerged in the liquid will cause multiple related domains to occur in the actual cleaning process. Thus, using the nonlinear wave equation, the P in (3), and p in (4) cannot be ordinarily solved. In acoustic application, the HRA will be used here to calculate $\{u\}$ based on the finite element method and the Navier-Stokes equations [21], [26], [27]. In the HRA, the system will be composed of two fluid domains as air and water, two solid domains as stainless steel and aluminum alloy, one PZT domain as PZT8, two interfaces as solid/fluid interface, and solid/PZT8 interface. All domains and interfaces can be illustrated as in Fig. 2. In Fig. 2, each domain and interface materials are also defined, such as water as cleaning fluid, stainless steel as back mass and bolt, while the aluminum alloy is defined as front mass and other parts, including a cover of the SUT. The PZT8 has represented the piezoelectric material, and finally, the interfaces are defined, whereas the joint area between two different materials occurs. The reason behind the definition of these domains and interfaces is that $\{u\}$ at each area will be differently calculated, but all of them are connected and related.
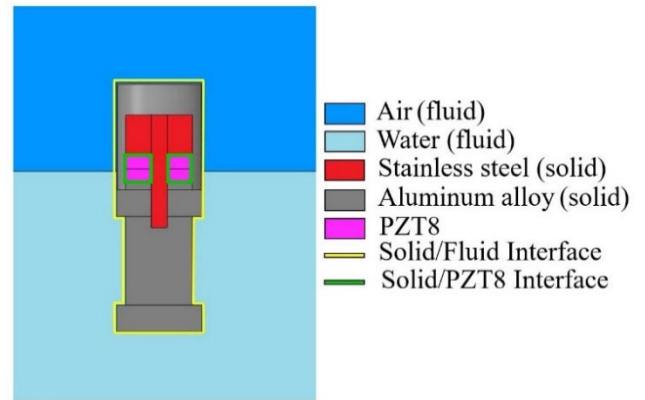

FIGURE 2. Illustration of domains and interfaces for Harmonic Response Analysis (HRA).

In the PZT8 domain and solid/PZT8 interface, when voltage (V) has been applied to the PZT8, the vibration is caused by coupling phenomena between structural and electric properties. Then $\{u\}$ can be figured out by (5) [26];

$$\begin{pmatrix} M_{uu} & 0 \\ 0 & 0 \end{pmatrix} \begin{Bmatrix} \ddot{u} \\ \ddot{V} \end{Bmatrix} + \begin{pmatrix} C_{uu} & 0 \\ 0 & -C_{vv} \end{pmatrix} \begin{Bmatrix} \dot{u} \\ \dot{V} \end{Bmatrix}$$
$$+ \begin{pmatrix} K_{uu} & K_{uv} \\ K_{vu} & -K_{vv} \end{pmatrix} \begin{Bmatrix} u \\ V \end{Bmatrix} = \begin{Bmatrix} F \\ Q \end{Bmatrix} \tag{5}$$

where $[M_{uu}]$ is a coupling mass matrix, $\{\dot{u}\}$ is a nodal velocity vector, $\{\ddot{u}\}$ is a nodal acceleration vector, $[K_{uv}]$ and $[K_{vu}]$ are piezoelectric coupling element matrix, and $\{V\}$ is a nodal voltage vector. $\{\dot{V}\}$, $\{\ddot{V}\}$ are 1st and 2nd derivatives of the nodal voltage vector. $[K_{uu}]$, $[K_{vv}]$ are structural stiffness and dielectric permittivity matrices, respectively. $\{F\}$ and $\{Q\}$ are force and electric loads, respectively.

When the wave of vibration travel to other domains, $\{u\}$ in (5) will also be transferred to those domains for calculating the response.

In the solid domain, $\{u\}$ from (5) will be calculated in (6) [5], [6], [27] as

$$[M]\{\ddot{u}\} + [C]\{\dot{u}\} + [K]\{u\} = \{F\} \tag{6}$$

while in the solid/fluid interface, $\{u\}$ from (5) will be calculated in (7) [21], [27] as

$$\left(-\omega^2 \begin{bmatrix} M_S & 0 \\ \rho R^T & M_F \end{bmatrix} + j\omega \begin{bmatrix} C_S & 0 \\ 0 & C_F \end{bmatrix} + \begin{bmatrix} K_S & -R \\ 0 & K_F \end{bmatrix} \right)$$
$$\times \begin{Bmatrix} u \\ p \end{Bmatrix} = \begin{Bmatrix} F_S \\ F_F \end{Bmatrix} \tag{7}$$

where $[R^T]$ is an acoustic mass matrix. The subscripts of S and F refer to structure and fluid, respectively. $\{p\}$ is an acoustic pressure vector.

In the fluid domain, considering p as an acoustic wave that can be linearly propagated through medium and pressure can be written as time-harmonic relation as $p = p_0 e^{j\omega t}$, p can be calculated using the HRA of ANSYS software. The HRA is equipped with the Navier-Stokes equations to calculate p in various domains, whereas p of the fluid domain in (4) will be changed to the acoustic domain using the Galerkin procedure. In Galerkin procedure, (4) will be multiplied with testing function (w) then integrated all over its volume to be as (8), which can provide $\{p\}$ as [21], [27]

$$\left(-\omega^2 [M_F] + j\omega[C_F] + [K_F] \right) \{p\} = \{F_F\} \tag{8}$$

When materials properties and boundary conditions are all defined, the software will find the numerical solution of (1), (4)-(8) and provide $\{p\}$ in the water domain, then plotted in graphical color for analysis purposes. Please be noted that (1) and (8) are in similar forms but situated on the different domains where (1) and (8) are in the structural and acoustic domains, respectively.

III. METHODOLOGY

A. SUBMERSIBLE ULTRASONIC TRANSDUCER
The 50 kHz SUT is used as a case study since it is a standard frequency and has many applications for ultrasonic purposes available in this frequency range. The SUT can be shown as in Fig. 1 (b). When the cover is removed, the front mass, piezoelectric materials, and back mass will be revealed. For the 50 Watt and 110 V SUT, the front mass is made of aluminum alloy in a dual-stepped design. The piezoelectric material is PZT8 type, and the back mass is stainless steel, as shown in Fig. 2. The cover also is made of aluminum alloy installed at the back to hide the PZT8 part, back mass, and electronic circuit. When this SUT is placed into the liquid and applied with electricity, all components will vibrate, cause the cleaning process, and affect bacteria growth.

B. MODELS
The original SUT has been used to create a CAD model in a computer simulation then mesh models will be created for the structural and acoustic simulations, respectively. For the structural simulation, Fig. 3 (a) and (b) show the solid
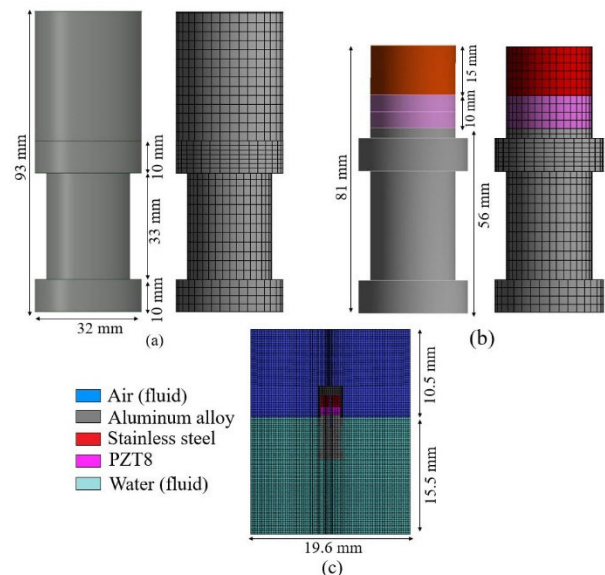

FIGURE 3. Solid mesh models of SUT: (a) outer, (b) inner for structural simulation, and (c) included fluid mesh models of air and water for acoustic simulation.

and mesh models of outer and inner when the cover is removed, respectively. The dimensions of the models also are mentioned in Fig. 3. For the acoustic simulation, the setup of the mesh model for the SUT submerged into the water at 5 cm depth in the tank of $95 \times 196 \times 155$ m^2 (W×L×H) has been created as shown in Fig. 3 (c). In this mesh model, the meshes of water and air have been included. Both mesh models are set to be hexahedrons with the size of 3 mm. The 3 mm refers to requiring one wavelength to be at least six elements [7], [21]. Using the equation $v = f\lambda$, the wavelength is 3 cm; therefore, the largest acceptable mesh size to give credible results is 5 mm. This research set the mesh size at 3 mm, smaller than the requirement to achieve highly accurate results. After the mesh independent analysis, we found that the suitable mesh model for the structural simulation is 33,054 nodes and 7,010 elements, while the maximum skewness is 0.81. For the acoustic simulation, the suitable mesh models have mesh ranges of 110,508-193,840 nodes and 22,270-44,835 elements with the maximum skewness below 0.86, depending on the simulation circumstance.

C. BOUNDARY CONDITION AND SETTINGS
The specification and behavior of SUT's vibration have been carefully investigated. The recorded values have been adopted into the settings and boundary conditions of the simulation as mentioned in Fig. 4 for (a) solid domain, (b) piezoelectric domain, and (c) fluid domain. The setups of interfaces are defined as in Figs. 2-4. In the structural simulation, the HRA has been set to calculate the natural frequency and response in the range of 45-55 kHz, which is expected to be the optimum value of SUT's vibration. For the acoustic simulation, the SUT has been set its positions in the water at 3 values of depth: 1 cm, 2.65 cm, and 5.3 cm, respectively. The HRA has been employed to calculate the
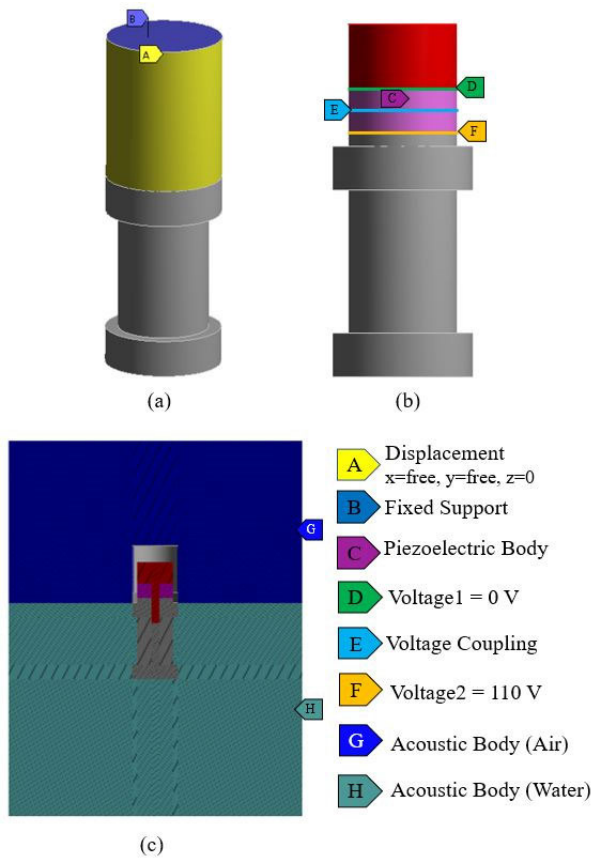
FIGURE 4. Settings and boundary conditions of the SUT simulation for (a) solid domain, (b) piezoelectric domain, and (c) fluid domain.

FIGURE 5. LDV experimental setup: (a) LDV machine, and (b) sampling points for measurement.

acoustic pressure at various positions in the 2.8-liter tank at 25 °C with the sound velocity in the water at 1,507 m/s. Numbers of mesh and elements in all 3 depth positions are mentioned in section IIIB. In this research, when the development of the SUT has been studied, the original PZT8 has been replaced with the PZT4. This change can cause a higher efficiency of cleaning where other parameters remain identical. The material properties of PZT8 and PZT4, including related parameters, were defined as in [4], [7]. The details and results of this change will be described later.

D. EXPERIMENT

Experiments can be divided into the LDV experiment, power concentration measurement, and plate counting method. For the LDV experiment, the SUT will be installed as in Fig 5 (a). Noted that, the LDV experiment was generally designed to measure the vibration of the small piece of electronic parts. Therefore, using the LDV to measure the vibration of the SUT, which is about 50 times larger, will confront the limitation of operation. However, the LDV setup has been modified to measure vibration amplitudes on SUT at three points (P_1, P_2, and P_3), as shown in Fig. 5 (b). Referring to coordinates of simulated amplitudes, the measurable vibration in this experiment is consistent with directional deformation in the y-axis of the system. While the vibration is
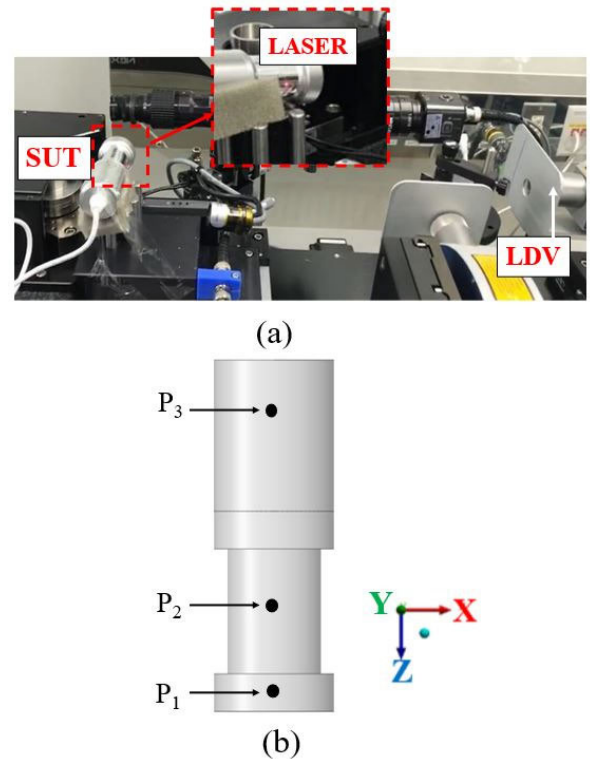
measured as shown in Fig. 5 (a), the LDV would expose scanning-frequency laser from 45-55 kHz to the three sampling points on the SUT's surface. With resonance phenomena and the Doppler effect, the LDV can detect the vibration amplitude at each point as a function of frequencies. These measurable amplitudes will be compared to the results from the structural simulation later.

Fig. 6(a) demonstrated power concentration measurement using the NGL measurer (model UPC 30000) measured the 2.8-liter tank. The resolution of the NGL measurer is ±0.1% W/liter. 5 sampling points have been determined named P_1-P_5 where P_1-P_3 aligned on the side of SUT and under the water surface at 1.0, 4.6, and 7.7 cm, respectively. P_4 and P_5 are on the middle line under the head of the SUT and the water surface at 1.2 and 8.0 cm, respectively. Each sampling point will be repeatedly measured 5 times.

To confirm the effect of ultrasonic waves in the inhibitory activity of pathogenic bacteria: *Escherichia coli (E. coli), Salmonella typhi (S. typhi), Staphylococcus epidermidis (S. epidermidis)*, and *Staphylococcus aureus (S. aureus)*, each 0.5-liter of microorganism suspension containing approximately 109 CFU/mL of each bacteria was treated by ultrasonic for sonication times of 3 and 5 minutes. First, it was stirred, and then the samples were collected at different points of the tank. Next, serial dilutions were prepared, and 500 μL of sample solution diluted were spread in triplicate onto plate count agar, incubated 24 h at 37 °C to determine total bacterial counts as colony-forming unit
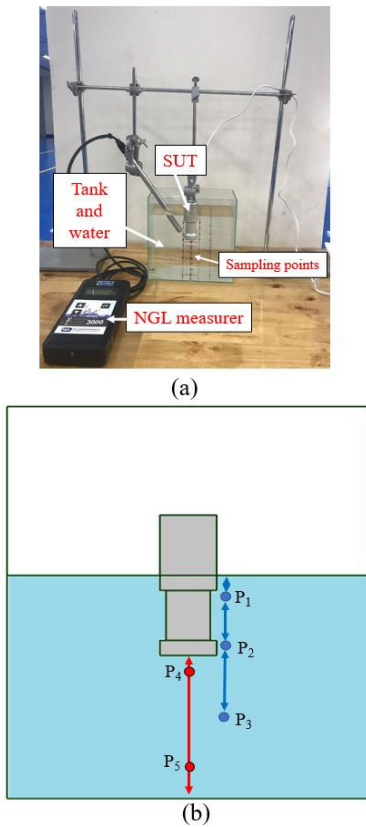
(a)

(b)

FIGURE 6. Power concentration experimental setup: measurement, and a schematic diagram displayed the investigated points.

FIGURE 7. Designs of front mass at various shapes such as reactor (original), stepped, conical, exponential, hyperbolic, and modified reactor labelled as models A-F showed in (a) - (f), respectively.

FIGURE 8. A Flowchart of methodology.

per milliliter (CFU/mL). Last, the total numbers of colonies of the control and treated samples were measured with the plate counting method with some modifications, according to Zhang *et al.* [28]. Each experiment will be repeatedly tested three times.

E. PROPOSED MODELS OF SUT

The front mass shape of the SUT is commonly named dual-stepped shape. The shapes of the front mass [12]–[16] and the types of PZT [4], [17], [18] can directly affect the efficiency of the transducers. Therefore, to develop the efficiency of the cleaning process, this research proposed 5 models of the front mass shapes named dual-stepped (original), stepped, conical, exponential, hyperbolic, and modified dual-stepped as shown in Fig. 7 and labeled as model A – F, respectively. Noted that the model F is roughly identical to model A except only the width of the head of the model F is wider than the model A for 5 mm. Furthermore, each shape of the model has been replaced with its materials from PZT8 to PZT4 to investigate the change of the vibration. From the acoustic simulation, the HRA has been employed to examine the acoustic pressure when the shapes of the front mass and the types of the PZT have been altered. The mesh models and the boundary conditions have been defined to mimic the use of ultrasonic in the inhibitory growth of pathogenic bacteria. All results of the simulation are comparable to the figure of the optimized
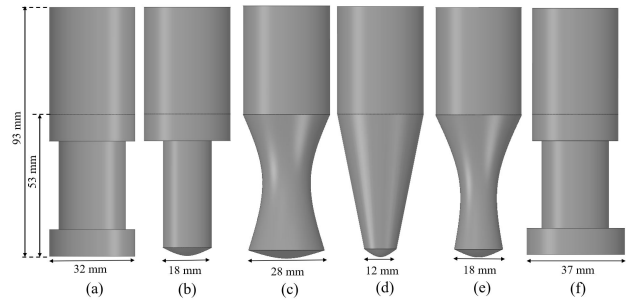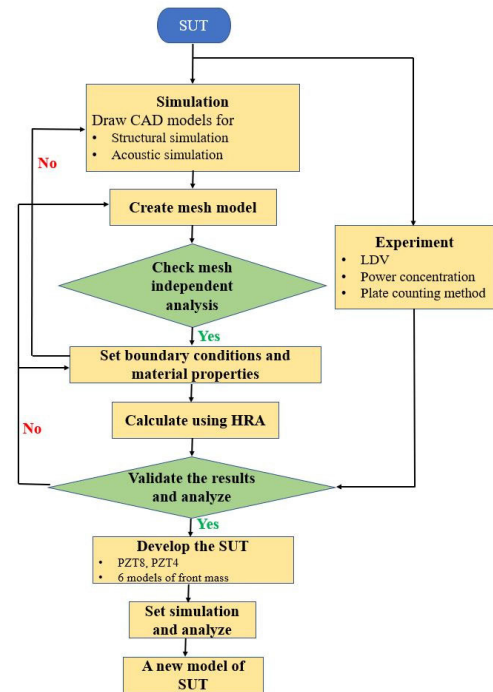
design of the SUT with higher efficiency. The methodology of the research can be concluded as a flowchart as in Fig. 8.

IV. RESULTS AND DISCUSSION

A. VIBRATION ANALYSIS, VALIDATION, AND INHIBITORY GROWTH OF PATHOGENIC BACTERIA

In Fig. 9, comparative results from the LDV experiment and the structural simulation using the HRA have been expressed and revealed the frequencies and vibration amplitudes at (a) P_1, (b) P_2, and (c) P_3, respectively. The results are well consistent in both experiment and simulation. In terms of frequencies, all sampling points exhibit the 50 kHz vibration, which corresponds to the natural frequency of the SUT as in an expected specification. The other peaks may rise from the error in the experiment as the LDV measurement has been modified its setup. If the LDV specifically designed for the SUT has been applied in the experiment, all other peaks
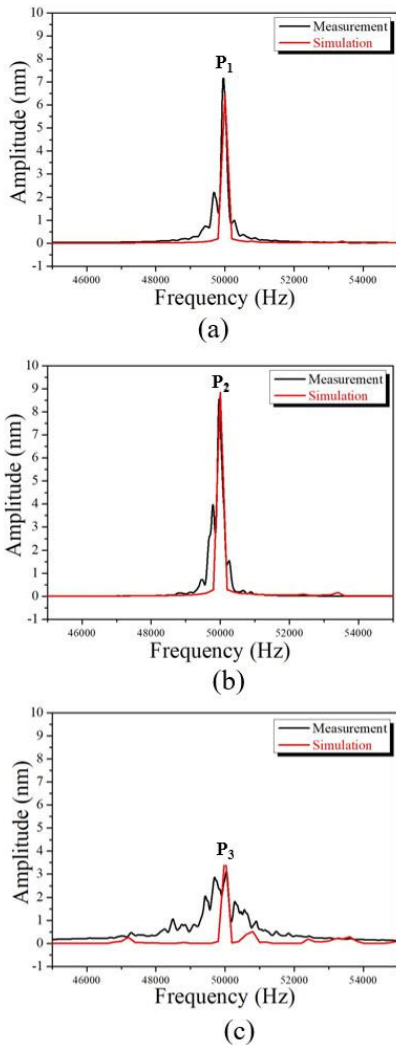
FIGURE 9. Relation between the frequency and vibration amplitude from both HRA simulation (red) and LDV measurement (black) comparable at (a) P_1, (b) P_2 and (c) P_3.

FIGURE 10. Deformation of (a) directional deformation in y-axis, (b) total deformation considering from the outside viewing (with cover), and (c) total deformation considering from the inside viewing (cover removed).

further than 50 kHz will be eliminated. From the amplitude point of view, both experiment and simulation gave the result with high consistency. The difference between the measurement and simulation results is also caused by the limitation of LDV measurement as described in IIID. Furthermore, considering the measurable values, the simulation provided the amplitudes with error at 9.7%, 3.6%, and 25.8% for P_1, P_2, and P_3 positions, respectively, showing the calculation's good performance. For such a higher error at P_3, it may be from the cause of unsuitable clamp of SUT, which gave rise to the larger error of measurement as the sampling point situated at a higher level as in Fig. 5.

The results from the structural simulation at other positions also exhibit the directional deformation in the y-axis, which aligned at the same axis to the LDV detector, total deformation considering from the outside viewing (with cover), and total deformation considering from the inside viewing (cover removed). The results are graphically plotted as in Fig. 10(a), (b), and (c), respectively. The results
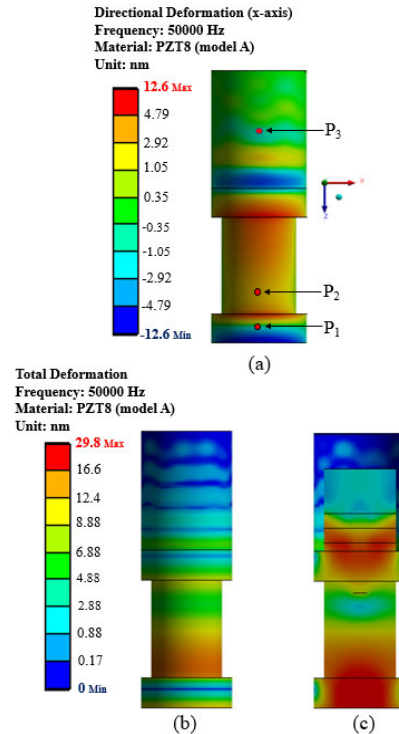
in Fig. 10 (a) and (b) also are consistent with the result in Fig. 9 as the horizontal vibration (y-axis) showed more substantial evidence at the middle (P_2) and the head (P_1) of the SUT while the tail (P_3) will have the smallest vibration. To investigate the effect of vibration, the total deformation in Fig. 10(c) has been compared to the materials' positions in Fig. 3(b). When the current has been applied to the SUT, the PZT8 will drastically vibrate to the front mass. Since the front mass is made of aluminum alloy, it has a comparatively low density than the back mass, made of stainless steel. This vibration has been utilized in various applications mentioned in section I, consistent with the purpose of the SUT design. In the front mass, it can be seen that the vibration will gradually increase from the position next to the PZT8 and rise to the highest at the head of the SUT. The behavior of vibration discovered here was consistent with the results reported in [12-.15], even though the shapes of the front mass are different from this research. The consistencies of the results in Figs. 9 and 10 can confirm that the structural simulation and methodology are reliable.

In Fig. 11, the comparative of the power concentration measured by NGL measurer and the maximum negative (−max) acoustic pressures calculated by the HRA at P_1, P_2, and P_3 positions when the SUT has been submerged into the water at (a) 1.00 cm, (b) 2.65 cm, and (c) 5.30 cm, respectively have been plotted. Both values
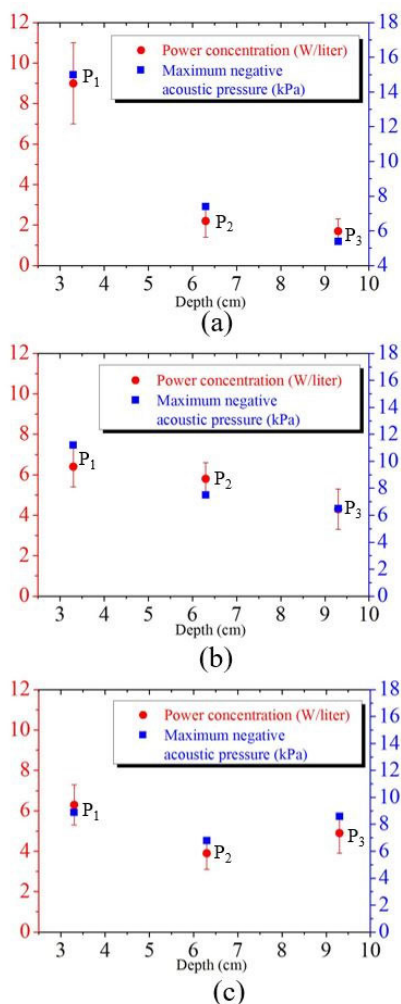
FIGURE 11. Comparative of the power concentration and the maximum negative acoustic pressure at P_1, P_2 and P_3 positions when the SUT has been submersible into the water at (a) 1.00 cm, (b) 2.65 cm and (c) 5.30 cm.

exhibit great consistency. Furthermore, the results showed that the further position from the SUT, the fewer values of the power concentration, and the −max acoustic pressure occur. The exception happened in P_3 of Fig. 11(c), as both values are increased. Because the SUT has been submerged at the 5.3 cm depth, which is closest to the bottom of the tank, the ultrasonic wave generated from the SUT can travel to the bottom and reflected, forming superimposed waves caused by the higher values in Fig. 11(c). This phenomenon cannot be seen in the larger tank in [3]–[7] with 10-20 liters capacity. This event only happens in the tank of 2.8 liters in this research. For further discussion, the smaller tank size can cause the superimposed ultrasonic wave to occur and give rise to a higher level of acoustic pressure, especially at the positions near the wall of the tank. Therefore, the design of such a small ultrasonic cleaning tank should carefully consider the superposition of the ultrasonic wave, which may cause damage to the cleaning object. This phenomenon has not been reported elsewhere. From the consistencies of all

results and well-considered in Physics, we can conclude that the acoustic stimulation and the methodology are credible.

To confirm the effect of vibration from the SUT in the inhibitory growth of pathogenic bacteria, Table 1 revealed the antimicrobial effect of ultrasonic waves generated by the SUT in the culture medium for 3 and 5 mins. The results showed that SUT vibration with 50 kHz produced a 6 μm [29] cavitation bubbles radius and affected bacterial viability, especially in *E. coli*. Furthermore, there is a significant reduction of total viable cell count between untreated and treated with the ultrasonic cleaner. A literature review [30] found that *E. coli* and *S. typhi* are rod-shaped with an average size of 1.1-1.5 μm width and 2.0-6.0 μm long. *S. typhi* is more diminutive than *E. coli*. On the other hand, *S. epidermidis* and *S. aureus* are spherical with an average diameter of 0.5-1.5 μm, more petite than *E. coli, S. typhi,* and significantly smaller than bubble size of 6 μm. In fact, since the cleaning process is effective, the particle size is close to the bubble size. Similarly, the bubble size closed to the bacteria size gives effective inhibitory growth. Therefore, our results of the plate counting method also corresponded to the fact. Increasing the repeated time of the experiment and using the proper ultrasonic cleaning conditions for each bacteria type will reduce the error and help all data be significant. Although the reduction is not significant in other pathogens (*S. typhi, S. epidermidis, and S. aureus),* it can still confirm that the SUT and bubble size affected bacterial cells growth. From (2) and reported in [8], our results imply that the inhibitory growth of pathogenic bacteria depends on frequency, cleanser, bubble size, acoustic pressure, fluid type, front mass's shape, PZT type, etc. Therefore, different microorganisms might require other conditions to operate the ultrasonic transducer.

To investigate the efficacy of the SUT, a SUT with titanium stepped front mass with a diameter of 10 mm operating at 28 kHz, 300 W in [31] was studied. It was installed with other accessories and then was submerged directly into the microorganism suspension for 10, 20, and 30 minutes for sonication times. The results revealed that the sonication of 10 min resulted in an average value of significant reduction for *E. Coli* cells of 2.75 log$_{10}$CFU. Other sonication times showed no significant difference, consistent with our results. When the mentioned significant reduction in [31] was compared to 2.64 of 3 min and 2.84 of 5 mins in Table 1, the result of comparison implied that the dual-stepped SUT and frequency employed in this work offers higher efficacy in the inhibitory of *E. Coli* than the stepped SUT in [31] because of shorter sonication time usage. Moreover, the dual-stepped SUT of this research is cheaper, easier to move, and does not require other accessories to use.

B. DEVELOPMENT OF SUT
For further development of the SUT, all models of the front masses in section IIIE have been investigated in terms of the acoustic simulation for a 2.8-liters tank using PZT8 as the piezoelectric material. The boundary conditions and the other settings have been assigned to mimic the circumstance of the

TABLE 1. The total variable count of the pathogenic bacteria between untreated and treated experiments with the ultrasonic cleanser at different times.

Time (mins)	Microorganism reduction ($\log_{10}$ CFU)							
	Escherichia coli		*Salmonella typhi*		*Staphylococcus epidermidis*		*Staphylococcus aureus*	
	Untreated	Treated	Untreated	Treated	Untreated	Treated	Untreated	Treated
3	11.44[a]	8.80[b]	10.40[c]	9.50[d]	14.17[c]	13.89[d]	14.47[c]	14.20[d]
5	11.44[a]	8.60[b]	10.40[c]	9.80[d]	14.17[c]	13.85[d]	14.47[c]	14.25[d]

All data are means of determination with standard deviation (±)

[a,b] Data between untreated and treated are given as means ± SD with different letters in the same row are significantly different (P < 0.05).

[c,d] Data between untreated and treated are given as means ± SD with different letters in the same row are not significantly different (P > 0.05).

FIGURE 12. Distribution of acoustic pressure in the tank using PZT8 as the piezoelectric material (a-f) for models A-F.
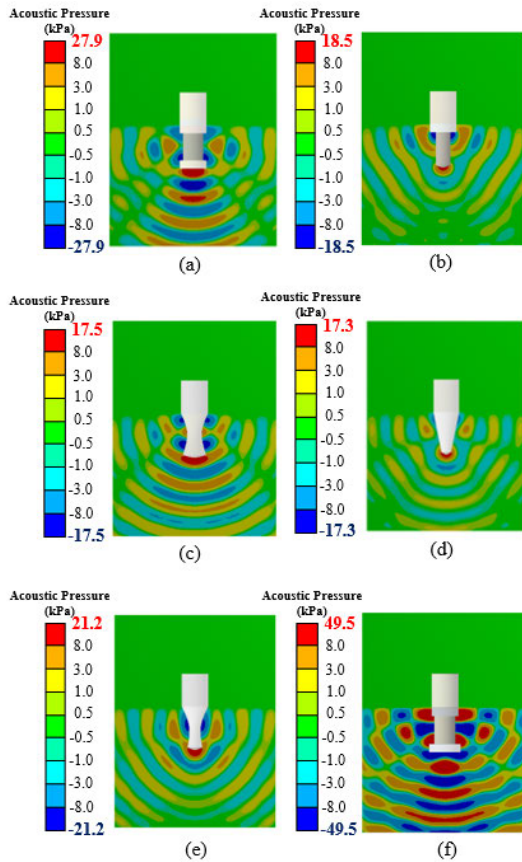

FIGURE 13. Distribution of acoustic pressure in the tank using PZT4 as the piezoelectric material (a-f) for models A-F.

SUT usage in the inhibitory activity of pathogenic bacteria, as in Table 1. The simulation results calculated by the HRA can be shown as in Fig. 12(a) – (f) for the models A-F, respectively. As in Fig. 12, the vibration at the tail is obviously less than other positions at the middle and the head of the SUT. Moreover, the tail of SUT is surrounded by air whose density is much less than the water, representing the media effect of the vibrational generating. In addition, the materials also play an important role as the density of the material of the back mass is higher than the front mass. These parameters caused that there is no acoustic pressure distributed on top of the SUT. In contrast, the acoustic pressure distribution can be clearly observed at the submerged region of the SUT that is in the water. The result is in good agreement with the conceptual design of the manufacturer. The plots in Fig. 12 also
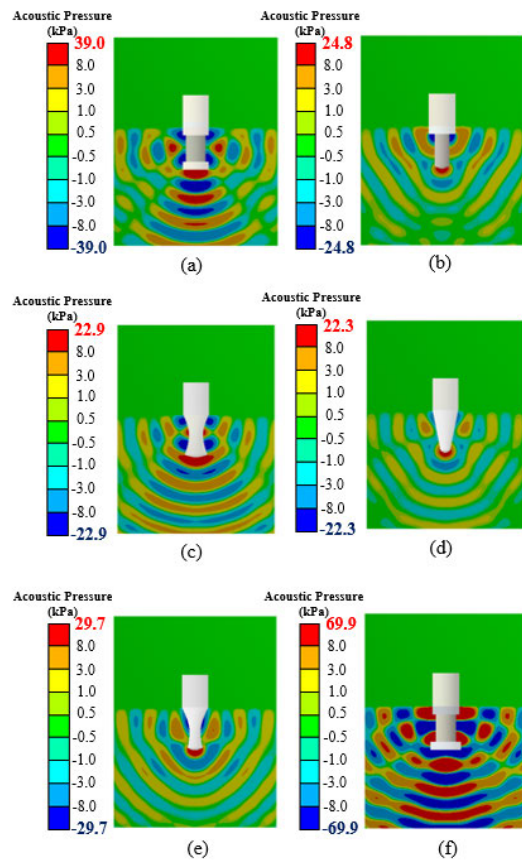
exhibit the severe vibration around the head (P_1) and the middle (P_2) of the SUT, consistent with the LDV experiment results described in Fig. 9. Moreover, the result revealed that the shape of the front mass produces a significant effect on the acoustic pressure distribution around the SUT. Model F in Fig. 12(f) performed the maximum negative and positive (±max) acoustic pressure, which was also 77.2% higher than the values in model A in Fig. 12 (a). Model F also provides the distribution of the acoustic pressure through to all over the tank. On the other hand, the designs of the front mass in Fig. 7 (b)-(e) gave rise to the lower level of vibration, which decreases the acoustic pressure at every point of the tank.

Likewise, Fig. 13 demonstrates the acoustic simulation in similar conditions, except only the PZT8, has been replaced by the PZT4. The simulation results calculated by the
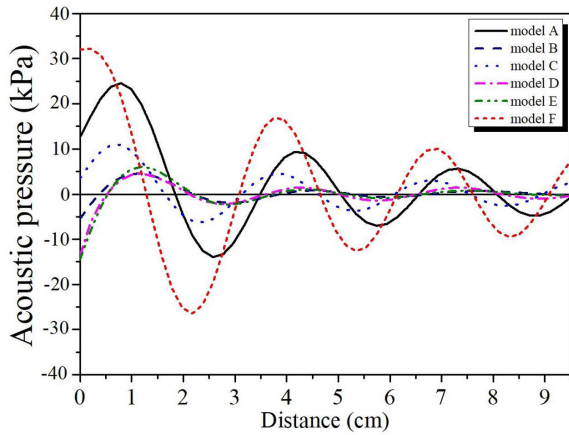
FIGURE 14. Acoustic pressure along the line between positions P_4 and P_5 retrieved from Fig. 13.

TABLE 2. ±Max acoustic pressure and percentage of increment recorded from Figs.13 and 14.

Model	±Max of Acoustic pressure (Pa)	
	PZT8 (from Fig.12)	PZT4 (from Fig.13)
A	27,945 (0.0%)	39,023 (+39.6%)
B	18,478 (-33.9%)	24,794 (-11.3%)
C	17549 (-37.2%)	22,905 (-18.0%)
D	17,264 (-38.2%)	22,270 (-20.3%)
E	21,198 (-24.1%)	29,687 (+6.2%)
F	49,508 (+77.2%)	69,943 (+150.2%)

FIGURE 15. Structural simulation of the SUT from Fig. 14 (f) for (a) the directional deformation in y-axis with cover, (b) the total deformation with cover and (c) the total deformation without cover.

HRA revealed that all designs of the front mass using the PZT4 produced the acoustic pressure distribution in the same way as the usage of the PZT8 but at a higher level of magnitude. Focusing on model F in Fig. 13(f), the acoustic pressure occurred and was distributed all over the tank, resulting in ±max acoustic pressure with 150.2% higher than the original design in model A of Fig. 12(a). All mentioned results of ±max acoustic pressure in Figs. 12 and 13, including their increment percentages compared to model A in Fig. 12(a), are reported in brackets of Table 2.

To investigate the effect of the front mass shape on the acoustic pressure in the cleaning tank, Fig. 14 plotted the acoustic pressure along the line between positions P_4, and P_5 retrieved from Fig. 12. In this plot, the character of the sinusoidal wave of the acoustic pressure has clearly been revealed. In all models, the generated waves have an identical wavelength at 3 cm, corresponding to the recalculated frequency at 50,233 Hz. This frequency is approximate to the designed SUT manufacturer value at 50,000 Hz with a 0.47% error. Even though the generated waves' character is undifferentiated, the amplitudes vary in magnitudes, and the phase shift can be found. As the distance from the head of the SUT gets larger, the acoustic pressure amplitudes will be decreased. This matter corresponds to the actual cleaning process using SUT as if the object is placed further away from the SUT, the cleaning tends to be less efficient. This investigation also was conducted to the result in Fig. 4,
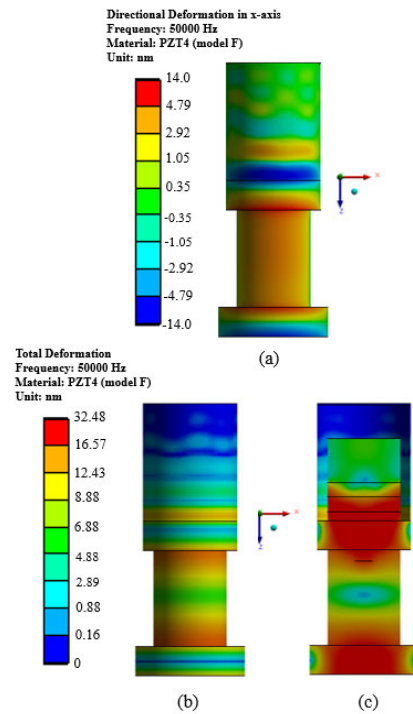
which used PZT4 as the materials. The results are parallel to the discussions of Fig. 14, except that the wave's amplitudes using PZT4 are higher than the usage of the PZT8 by 3.1%-9.3%, depending on the model. These results were consistent with the results reported in Ref. [4,18] that the PZT4 gives a higher electric response than PZT8. The model F using the PZT4 can generate the highest value of the acoustic pressure; therefore, this model can be an interesting candidate for further investigation later.

Fig. 15 presents the structural simulation of the SUT from Fig. 13(f) for (a) the directional deformation in the y-axis with cover, (b) the total deformation with cover, and (c) the total deformation without cover. Comparable to Fig. 10 (a), we found that the change of the front mass shape and the PZT's type in Fig. 15 (a) lead to higher intensity of the vibration in the horizontal direction up to 11.1% and the total deformation in Fig. 15 (b) and (c) is higher than that in Fig. 10 (b) and (c) up to 9.0%.

From Figs. 12-15, it can be indicated that the change of the front mass shape as the model F and using the PZT4 as the piezoelectric can lead the SUT to produce the stronger vibration with higher acoustic pressure fully distributed throughout the tank than the original design.

As seen in (2), the surface tension (σ) the fluid density (ρ) are two parameters that affect the cavitation. The manufacturers employ surfactant and ultrasonic cleaning fluid to reduce the surface tension and fluid density in actual use. This action increases f_0 in (2), accelerating the generation

of cavitation effect and increasing the number of cavitating bubbles. The surfactant is a chemical, while the ultrasonic cleaning fluid is a mixture of deionized (DI) water and chemical. The formulations, ingredients, and properties are secrets of each company that is often not disclosed. Since the acoustic pressure is strongly related to cavitation, the efficiency of the cleaning process in [3-.7], and the inhibitory activity of pathogenic bacteria [8.,9], adding the surfactant and using the suitable ultrasonic cleaning fluid into the experiment will optimize the inhibitory growth efficiency of bacteria. Thus, this research's final proposed model and methodology can be exploited to develop the next generation SUT. Also, they can be modified to be a cell disruptor device with higher efficiency in the cleaning process and can inhibit pathogenic bacteria, especially *E. coli*. Therefore, the future challenge of work would be how to design the front mass shape and find out the operational condition that exhibits the highest cleaning efficiency and inhibit other pathogenic bacteria.

V. CONCLUSION

To develop the next generation of the SUT with higher efficiency of cleaning and also capable of inhibiting the growth of the pathogenic bacteria, this research used HRA to investigate the vibration and cleaning process of the original version of the SUT at 50 kHz, 50 W, and 110 V. This model of the SUT equipped with the dual-stepped front mass and the PZT8 as the piezoelectric material. The result of the structural simulation exhibits the vibration at 50 kHz corresponding to the natural frequency of this SUT. The investigation also reveals that the vibration at the head and the middle of SUT are higher than that at the tail. This discovery has been confirmed to the actual measurement of the frequency and vibration amplitude using the LDV. In detail, the vibration severely occurs at the head of the front mass, consistent with the previous report. The acoustic simulation showed strong vibration at the head and the middle of the SUT. For the tail part, the vibration decreases corresponding to the actual measurement using the NGL measurer. When this SUT has been conducted to inhibit pathogenic bacteria, the results show that the SUT's vibration affected bacterial viability, especially in *E. coli*. For the development part of the SUT, this research investigates 5 front mass shapes, e.g., dual-stepped (original), stepped, conical, exponential, hyperbolic, and modified dual-stepped equipped with the PZT4. Using the structural simulation to investigate the vibration and the acoustic simulation to explore the cleaning process of the SUT. The results conclude that the change of the front mass shape and type of the PZT alter the amplitude and phase of vibration but steady the wavelength of the vibration. The simulation also showed that the further position away from the SUT, the amplitude will be decreased. The head of the original front mass is modified to be wider at 5 cm and using the PZT4 can cause severe vibration with higher acoustic pressure and be thoroughly distributed throughout the cleaning tank. These phenomena lead to the higher efficiency of cleaning than the original SUT. Finally, the research reveals the behavior of the vibration of

the SUT, the new model of the front mass, and the suitable methodology necessary to design the next generation of the SUT with higher efficiency for commercial purposes.

REFERENCES

[1] W. J. Yu, T. Yu, and S. J. Park, "Design of the metal-welder ultrasonic transducer by using finite element analysis," *Appl. Mech. Mater.*, vol. 511, pp. 1117–1144, Mar. 2014.

[2] M. T. Taylor, G. T. A. Kovacs, P. Belgrader, R. Joshi, S. Sakai, M. A. Northrup, and K. E. Petersen, "Disrupting bacterial spores and cells using ultrasound applied through a solid interface," in *Proc. 2nd Annu. Int. Special Topic Conf. Microtechnol. Med. Biol.*, Madison, WI, USA, May 2002, pp. 551–555.

[3] W. Tangsopha, J. Thongsri, and W. Busayaporn, "Simulation of ultrasonic cleaning and ways to improve the efficiency," in *Proc. Int. Elect. Eng. Congr. (iEECON)*, Pattaya, Thailand, Mar. 2017, pp. 1–4.

[4] W. Tangsopa, T. Keawklan, and K. Kesngam, "Improved design of ultrasonic cleaning tank using harmonic response analysis in ANSYS," *IOP Conf. Ser., Earth Environ. Sci.*, vol. 159, Oct. 2018, Art. no. 012042.

[5] W. Tangsopa and J. Thongsri, "Development of an industrial ultrasonic cleaning tank based on harmonic response analysis," *Ultrasonics*, vol. 91, pp. 68–76, Jan. 2019.

[6] W. Tangsopa and J. Thongsri, "A novel ultrasonic cleaning tank developed by harmonic response analysis and computational fluid dynamics," *Metals*, vol. 10, no. 3, p. 335, Mar. 2020.

[7] W. Tangsopa and J. Thongsri, "A dual frequency ultrasonic cleaning tank developed by transient dynamic analysis," *Appl. Sci.*, vol. 11, no. 2, p. 699, Jan. 2021.

[8] S. E. Bilek and F. Turantas, "Decontamination efficiency of high power ultrasound in the fruit and vegetable industry, a review," *Int. J. Food Microbiol.*, vol. 166, no. 1, pp. 155–162, 2013.

[9] N. D. S. Cruz-Cansino, I. Reyes-Hernández, L. Delgado-Olivares, D. P. Jaramillo-Bustos, J. A. Ariza-Ortega, and E. Ramírez-Moreno, "Effect of ultrasound on survival and growth of escherichia coli in cactus pear juice during storage," *Brazilian J. Microbiol.*, vol. 47, no. 2, pp. 431–437, Apr. 2016.

[10] T. Wu, X. Yu, A. Hu, L. Zhang, Y. Jin, and M. Abid, "Ultrasonic disruption of yeast cells: Underlying mechanism and effects of processing parameters," *Innov. Food Sci. Emerg. Technol.*, vol. 28, pp. 59–65, Mar. 2015.

[11] D. Millan-Sango, E. Garroni, C. Farrugia, J. F. M. Van Impe, and V. P. Valdramidis, "Determination of the efficacy of ultrasound combined with essential oils on the decontamination of Salmonella inoculated lettuce leaves," *Lwt*, vol. 73, pp. 80–87, Nov. 2016.

[12] A. S. Nanu, N. I. Marinescu, and D. Ghiculescu, "Study on ultrasonic stepped horn geometry design and FEM simulation," *Rev. Tehnol. Neconventionale*, vol. 15, no. 4, p. 25, 2011.

[13] S. Roy and Jagadish, "Design of a circular hollow ultrasonic horn for USM using finite element analysis," *Int. J. Adv. Manuf. Technol.*, vol. 93, nos. 1–4, pp. 319–328, Oct. 2017.

[14] A. S. Samanta and R. Arora, "Structural analysis of horn used in ultrasonic enhanced oil recovery," *Indian J. Sci. Technol.*, vol. 11, p. 28, Jul. 2018.

[15] Y. Xuan, A. Wang, and N. Zhang, "Design and simulation technology of piezoelectric ultrasonic transducer with sandwich composite horn," *IOP Conf. Ser., Mater. Sci. Eng.*, vol. 470, Oct. 2019, Art. no. 012043.

[16] J. Yang, S. Ji, J. Zhao, and Q. He, "Theoretical analysis and finite element calculation of ultrasonic horn," *IOP Conf. Ser., Mater. Sci. Eng.*, vol. 612, Oct. 2019, Art. no. 032032.

[17] K. Nakamura, *Ultrasonic Transducers: Materials and Design for Sensors, Actuators, and Medical Applications*. Cornwall, U.K.: Padstow, 2012.

[18] D. A. DeAngelis and G. W. Schulze, "Performance of PZT8 versus PZT4 piezoceramic materials in ultrasonic transducers," *Phys. Proc.*, vol. 87, pp. 85–92, Mar. 2016.

[19] Y. Yao, Y. Pan, and S. Liu, "Power ultrasound and its applications: A state-of-the-art review," *Ultrason. Sonochem.*, vol. 62, Apr. 2020, Art. no. 104722.

[20] A. Pak, "Determination of material properties components used in FEM modeling of ultrasonic piezoelectric transducer," *ADMT J.*, vol. 12, no. 2, pp. 75–81, 2019.

[21] *Harmonic Analysis*, ANSYS, Southpointe, FL, USA, 2016.

[22] B. Avvaru and A. B. Pandit, "Oscillating bubble concentration and its size distribution using acoustic emission spectra," *Ultrason. Sonochem.*, vol. 16, no. 1, pp. 105–115, Jan. 2009.

[23] R. E. Apfel, "Acoustic cavitation," *Methods Experim. Phys.*, vol. 19, pp. 355–411, Dec. 1981.

[24] M. F. Hamilton and D. T. Blackstock, *Nonlinear Acoustics*. San Diego, CA, USA: Academic, 1998, p. 55.

[25] G. W. Griffiths and W. E. Schiesser, *Linear and Nonlinear Waves*, vol. 4, no. 7. San Diego, CA, USA: Scholarpedia, 2011.

[26] *Piezo and MEMS ACTx R180*, ANSYS, Canonsburg, PA, USA, 2018.

[27] *Introduction to Acoustics*, ANSYS Europe, Canonsburg, PA, USA, 2017.

[28] L. Zhang, Z. Lu, Z. Yu, and X. Gao, "Preservation of fresh-cut celery by treatment of ozonated water," *Food Control*, vol. 16, no. 3, pp. 279–283, Mar. 2005.

[29] J. Fuchs, "Ultrasonics—Number and size of cavitation bubbles— CTG technical blog," CTG Tech. Blog, Arlington, TX, USA, Tech. Rep., Jun. 2021. [Online]. Available: https://techblog.ctgclean.com/2011/12/ultrsonics-number-and-size-of-cavitation-bubbles/

[30] S. Aryal. *Different Size, Shape and Arrangement of Bacterial Cells*. Accessed: Jan. 12, 2018. [Online]. Available: https://microbiologyinfo.com/different-size-shape-and-arrangement-of-bacterial-cells/

[31] A. Sarkinas, K. Sakalauskiene, R. Raisutis, J. Zeime, A. Salaseviciene, E. Puidaite, E. Mockus, and D. Cernauskas, "Inactivation of some pathogenic bacteria and phytoviruses by ultrasonic treatment," *Microbial Pathogenesis*, vol. 123, pp. 144–148, Oct. 2018.

BENJAMAPORN WONGANU received the B.Sc. degree in biology from Khon Kaen University, Thailand, in 2003, the M.Sc. degree in molecular genetics and genetic engineering from Mahidol University, Thailand, in 2006, and the Ph.D. degree in bioengineering from Lehigh University, USA. She had experience as a research consultant of an industrial factory involving sterilizer machines. She is currently an Instructor with the Department of Biotechnology, Faculty of Applied Science, King Mongkut's University of Technology North Bangkok, Bangkok, Thailand. She has expertise in protein biotechnology, molecular genetic engineering, and molecular microbiology. She received a scholarship from the Development and Promotion of Science and Technology Talent Project during her study in the B.Sc. and M.Sc. degrees. For her Ph.D., she received the Ministry of Science and Technology Scholarship.

WUTTHIKRAI BUSAYAPORN received the B.Sc. degree in physics from Kasetsart University, Thailand, in 2002, the M.Sc. degree in physics from Chulalongkorn University, Thailand, in 2006, and the Ph.D. degree in materials science from The University of Manchester, U.K., in 2010. He is currently a Beamline Scientist with the Synchrotron Light Research Institute (Public Organization), Thailand, where he is also the Head of the Computational Materials Physics Project. He has expertise in first principle calculation and simulation of surface structure determination.

JATUPORN THONGSRI received the B.Sc. degree in physics from Khon Kaen University, Thailand, in 2002, and the M.Sc. and D.Sc. degrees in physics from Chulalongkorn University, Thailand, in 2005 and 2011, respectively.

He has expertise in computational fluid dynamics, finite element method, computer-aided design and manufacturing, and computer simulation. He is currently an Associate Professor in production engineering with the College of Advanced Manufacturing Innovation, King Mongkut's Institute of Technology Ladkrabang, Bangkok, Thailand. In addition, he is a researcher and a consultant of industrial factories who has experience in applying his expertise to solve problems and improve the manufacturing processes. He received a scholarship from the Development and Promotion of Science and Technology Talent Project throughout his study.

KAMONWAN SRATHONGHUAM received the B.S. degree in physics from Kasetsart University, Thailand, in 2019. She is currently pursuing the master's degree in advanced manufacturing system engineering with the College of Advanced Manufacturing Innovation, King Mongkut's Institute of Technology Ladkrabang, Thailand. Her research interests include finite element analysis and ultrasonic cleaning.

• • •